scientific reports

Check for updates

OPEN

Single-Cell RNA sequencing reveals mitochondrial dysfunction in microtia chondrocytes

Xinyu Li, Datao Li✉ & Ruhong Zhang✉

Microtia is a congenital malformation characterized by underdevelopment of the external ear. While chondrocyte dysfunction has been implicated in microtia, the specific cellular abnormalities remain poorly understood. This study aimed to investigate mitochondrial dysfunction in microtia chondrocytes using single-cell RNA sequencing. Cartilage samples were obtained from patients with unilateral, non-syndromic microtia and healthy controls. Single-cell RNA sequencing was performed using the 10 × Genomics platform. Bioinformatic analyses including cell type identification, trajectory analysis, and gene co-expression network analysis were conducted. Mitochondrial function was assessed through ROS levels, membrane potential, and transmission electron microscopy. Chondrocytes from microtia samples showed lower mitochondrial function scores compared to normal samples. Trajectory analysis revealed more disorganized differentiation patterns in microtia chondrocytes. Mitochondrial dysfunction in microtia chondrocytes was confirmed by increased ROS production, decreased membrane potential, and altered mitochondrial structure. Gene co-expression network analysis identified hub genes associated with mitochondrial function, including SDHA, SIRT1, and PGC1A, which showed reduced expression in microtia chondrocytes. This study provides evidence of mitochondrial dysfunction in microtia chondrocytes and identifies potential key genes involved in this process. These findings offer new insights into the pathogenesis of microtia and may guide future therapeutic strategies.

Keywords Microtia, Chondrocytes, Mitochondrial dysfunction, Single-cell sequencing

Microtia is a congenital malformation characterized by underdevelopment or absence of the external ear, affecting approximately 1 in 5,000 to 10,000 live births worldwide[1]. This condition not only impacts auditory function but also poses significant psychosocial challenges for affected individuals[2]. Despite its clinical significance, the underlying cellular and molecular mechanisms of microtia remain poorly understood, hindering the development of effective therapeutic strategies. Chondrocytes, the primary cell type responsible for cartilage formation and maintenance, play a crucial role in the development of the external ear[3]. Dysfunction of these cells has been implicated in various cartilage disorders, including microtia[4]. However, the specific cellular abnormalities in microtia chondrocytes have not been fully elucidated.

Mitochondria are essential organelles that regulate cellular energy metabolism, redox balance, and various signaling pathways[5–7]. Mitochondrial dysfunction has been associated with numerous developmental disorders and degenerative conditions[8–10]. When mitochondria fail to function properly, there is often an increase in the production of reactive oxygen species (ROS). Elevated levels of ROS can lead to oxidative stress, triggering inflammatory responses and activating cell death pathways, ultimately resulting in tissue damage and organ dysfunction[11–13]. This mechanism has been observed in numerous conditions, ranging from neurodegenerative diseases to metabolic disorders. This hypothesis is particularly compelling given the high metabolic demands of chondrocytes during cartilage formation and growth. Understanding the potential role of mitochondrial dysfunction in microtia could open new avenues for therapeutic interventions aimed at improving chondrocyte function and cartilage development in affected individuals. Given the high metabolic demands of chondrocytes during cartilage formation and growth, we hypothesized that mitochondrial abnormalities might contribute to the pathogenesis of microtia.

Department of Plastic and Reconstructive Surgery, Shanghai Ninth People's Hospital, Shanghai Jiao Tong University School of Medicine, Shanghai, China. ✉email: dataoli@163.com; zhangruhong@163.com

Methods

Sample preparation and inclusion criteria

Cartilage tissue samples were obtained from patients with unilateral, non-syndromic microtia who underwent auricular reconstruction surgery at our institution. The study was approved by the Institutional Review Board of our institution, and written informed consent was obtained from all participants or their legal guardians. The research was conducted in compliance with the principles of the Declaration of Helsinki. Microtia cartilage samples were collected from the auricular remnants of three patients with microtia. Additionally, normal ear cartilage samples were obtained from three healthy individuals undergoing otoplasty or other ear surgeries unrelated to microtia. The study was conducted according to the Declaration of Helsinki Principles. Immediately after surgical excision, the cartilage samples were washed with sterile phosphate-buffered saline (PBS) to remove blood and debris. The samples were then minced into approximately 1 mm^3 pieces using sterile surgical scissors. The minced tissue was enzymatically digested in a solution containing 0.2% collagenase II (Gibco, USA) in Dulbecco's Modified Eagle Medium (DMEM; Gibco, USA) at 37 °C for 16 h with gentle agitation. The resulting cell suspension was filtered through a 70 μm cell strainer (BD Biosciences, USA) to remove undigested tissue fragments. The filtered cells were then centrifuged at 300×*g* for 5 min at 4 °C, and the cell pellet was resuspended in PBS containing 0.04% bovine serum albumin (BSA). Cell viability was assessed using trypan blue exclusion, and only samples with > 80% viability were used for subsequent single-cell RNA sequencing. The cell concentration was adjusted to 1000 cells/μL for library preparation.

Library preparation and sequencing of scRNA

Following cell suspension preparation, single-cell RNA sequencing libraries were constructed using the 10 × Genomics Chromium Single Cell 3' Library & Gel Bead Kit v3 (10 × Genomics, Pleasanton, CA, USA) according to the manufacturer's protocol. Briefly, cell suspensions were loaded onto a Chromium Controller to generate gel beads in emulsion (GEMs). Within each GEM, cells were lysed, and the released mRNA was reverse-transcribed to cDNA using barcoded primers. After breaking the GEMs, the barcoded cDNA was amplified by PCR. The amplified cDNA was then fragmented, end-repaired, A-tailed, and ligated with adaptors. Finally, index PCR was performed to generate the final libraries. Library quality was assessed using an Agilent 2100 Bioanalyzer (Agilent Technologies, Santa Clara, CA, USA), and library quantification was performed using a Qubit 3.0 Fluorometer (Thermo Fisher Scientific, Waltham, MA, USA). The resulting libraries were sequenced on an Illumina NovaSeq 6000 platform (Illumina, San Diego, CA, USA) with paired-end 150 bp (PE150) reading strategy, aiming for an average of 50,000 reads per cell.

Data processing of 10 × scRNA-Seq

Single-cell RNA sequencing data analysis was performed using a combination of R packages and custom scripts. Initially, we utilized the Seurat package (v4.0.1) to import and process the 10 × Genomics scRNA-seq data. Quality control measures were implemented to exclude low-quality cells, including those with abnormally high or low gene counts, UMI counts, and mitochondrial gene percentages. Feature selection was conducted using the 'FindVariableFeatures' function in Seurat, identifying the top 2,500 variable genes. These genes were used for downstream dimensionality reduction and clustering analyses. We applied principal component analysis (PCA) followed by uniform manifold approximation and projection (UMAP) for visualization and cluster identification. To identify cluster-specific marker genes, we employed Seurat's 'FindAllMarkers' function with stringent criteria (|log2 fold change| > 0.5, minimum percentage expression > 0.22). For functional interpretation of the identified cell clusters, we conducted pathway enrichment analysis using the clusterProfiler package. This allowed us to understand the biological processes and molecular functions associated with each cell type or state.

Cell-type identification and differential abundance analysis

In our research, we employed a dual-approach strategy for cell type identification. Initially, we utilized the automated cell annotation tools SingleR and scCATCH to perform a preliminary classification of the cell clusters. Based on these initial results, we broadly categorized the cells into five main groups: chondrocytes, stromal cells, endothelial cells, stem cells, and immune cells. Subsequently, we refined our annotations by cross-referencing with published single-cell RNA sequencing datasets and analyzing the expression patterns of well-established cell-specific markers. We used miloR (version 3.15) to detect sets of cells that are differentially abundant in various conditions by modeling counts of cells in the neighborhoods of a k-nearest neighbor (KNN) graph. The log2 fold change of number of cells between two groups in each neighborhood was used for visualization.

Gene set score

Signature gene set scores were calculated for each cell using the Seurat AddModuleScore function. This method computes the average expression of a given gene set in individual cells, adjusting for background expression by subtracting the average expression of randomly selected control features. Positive scores indicate that the gene module is expressed at levels higher than expected based on the average population expression. Mitochondrial-related genes were identified by MitoCarta3.0 which contains an updated inventory of 1136 human mitochondrial genes[14].

Weighted gene co-expression network analysis

Weighted gene co-expression network analysis (WGCNA) is a robust and widely-validated technique for dimensionality reduction in complex datasets. This method clusters high-dimensional data into modules, effectively preserving the intrinsic relationships between variables within a network structure. WGCNA's strength lies in its ability to capture the nuanced interconnections among genes, providing a more comprehensive understanding of gene expression patterns and their potential functional implications[15]. High-dimensional

weighted gene co-expression network analysis (hdWGCNA) was employed to construct a scale-free network at the single-cell level using the R package 'hdWGCNA'. To ensure optimal network topology, we set the threshold for the scale-free topology model fit to exceed 0.85. After careful evaluation, a soft threshold of 12 was selected as it provided the best connectivity while maintaining the scale-free property of the network. Module-trait relationship analysis identified modules significantly associated with the mitochondria, and hub genes within significant modules were identified based on their intra-module connectivity. The hub genes were considered the key genes associated with high mitochondrial score.

Enrichment analysis

To elucidate the functional implications of the identified genes, we performed Gene Ontology (GO) enrichment analysis. This approach allowed us to characterize the biological pathways and molecular functions associated with these genes. Furthermore, to corroborate the relevance of these genes to mitochondrial activity, we conducted protein–protein interaction (PPI) network analysis. This additional step provided insights into the functional relationships and potential regulatory mechanisms among the identified genes, thereby strengthening the validity of our findings.

Trajectory analysis and gene set variation analysis

To infer the developmental trajectory of chondrocytes, we employed the VECTOR method as described by Zhang et al.[16]. This unsupervised approach leverages the observation that starting cells of a developmental lineage tend to have more polarized principal component values. This method uses principal component analysis and UMAP to process and visualize the single-cell RNA sequencing data. VECTOR identifies starting cells based on quantile polarization scores of principal component values, then computes pseudotime scores and developmental vectors for other cells in the UMAP space. This approach allows for unsupervised trajectory inference without relying on predefined marker genes. We conducted pseudotime analysis using Monocle2, employing the DDR-Tree algorithm with default settings. Prior to trajectory assessment, we carefully selected Seurat clusters for analysis, guided by established intercellular relationships reported in the literature. This comprehensive approach allowed us to reconstruct cellular differentiation paths and identify key genes involved in lineage decisions.

Measurement of ROS

Intracellular ROS levels were evaluated using the DCFH-DA fluorescent probe. DCFH-DA is a cell-permeable probe used to detect intracellular ROS[17]. Following the manufacturer's instructions (Biyuntian, shanghai, China), microtia chondrocytes and normal auricular chondrocytes were seeded in 6-well plates at a density of $5\times10^{\wedge4}$ cells per well. After cell adhesion, the cells were washed thrice with PBS and incubated with 10 μM DCFH-DA for 20 min at 37 °C in a light-free environment. After the incubation period, the cells were observed under a fluorescence microscope, and the intracellular ROS levels were quantified using ImageJ software.

Mitochondrial membrane potential (MMP)

Mitochondrial membrane potential (MMP) was assessed with the fluorescent probe JC-1 (Biyuntian, China) according to the manufacturer's instructions. The MMP was evaluated using the JC-1 fluorescent probe. Microtia chondrocytes and normal auricular chondrocytes were divided into two groups: the microtia group and the control group. Cells were seeded in 6-well plates at a density of $1\times10^{\wedge5}$ cells per well. After 24 h of culture, the supernatant was collected, and the cells were washed twice with PBS. Subsequently, 1 ml of JC-1 staining working solution was thoroughly mixed with the cells. The cells were then incubated at 37 °C for 20 min in a cell culture incubator[18]. After two washes with JC-1 buffer solution, the cells were supplemented with culture medium and examined and imaged under a fluorescence microscope. Red fluorescence indicates high MMP, while green fluorescence indicates low MMP. The ratio of green to red fluorescence intensity was calculated to assess the changes in MMP between microtia chondrocytes and normal auricular chondrocytes. Image analysis was performed using ImageJ software.

Histological staining

Auricular cartilage tissues were carefully dissected and fixed in 4% paraformaldehyde for 24 h at 4 °C. The tissues underwent standard dehydration through a graded ethanol series and were embedded in paraffin following conventional protocols. Paraffin Sects. (5 μm thickness) were prepared using a microtome. These sections were then dewaxed using xylene and rehydrated through a graded series of ethanol solutions (100%, 95%, 80%, 70%) and finally distilled water. For histological examination, two staining procedures were performed. First, sections were stained with hematoxylin and eosin using a standard staining kit (Beyotime, Shanghai, China) according to the manufacturer's instructions, allowing for visualization of overall tissue architecture and cellular morphology. Additionally, Safranin O-Fast Green staining was performed, where sections were stained with 0.02% Fast Green for 5 min, followed by three quick dips in 1% acetic acid, and then counterstained with 0.1% Safranin-O for 10 min. After staining, all sections were dehydrated through an ascending ethanol series, cleared in xylene, and mounted with a permanent mounting medium. The stained sections were then observed and imaged using a light microscope (Nikon Corporation) equipped with a digital camera. Multiple representative fields were captured for each sample to ensure comprehensive analysis of the tissue structure, cellular characteristics, and matrix composition.

Western blot assay

Total protein was isolated from human auricular cartilage tissue using RIPA lysis buffer (Beyotime, Shanghai, China). Protein concentration was determined using a BCA kit (Beyotime, Shanghai, China). Samples (20 μg/lane) were separated by SDS-PAGE and transferred to PVDF membranes (Merck-Millipore, Darmstadt,

Germany).The membranes were blocked with 5% non-fat milk for 2 h at room temperature, then incubated overnight at 4 °C with primary antibodies: SDHA, SIRT1, and PGC1A (all from Abcam, UK).After washing, the membranes were incubated with HRP-conjugated secondary antibodies for 2 h at room temperature. Protein bands were visualized using a chemiluminescence kit (Merck-Millipore, Darmstadt, Germany) and captured with a digital imaging system. Band intensities were quantified using ImageJ software.

Statistics and reproducibility

In cell experiments, each group contained more than 3 biological repeats, and the results for each sample were from the average of 5 different microscope fields. Analysis of the signal strength in the IHC images was performed using the IHC Profile plugin in ImageJ, and the positive score of each image was recorded and used for statistical analysis. In the quantitative analysis, each group contained more than 5 independent samples, and the results for each sample came from the average of three different microscope fields. Independent T-test were used for differential analysis. One-way ANOVA with Tukey's test were used to make pairwise comparisons among multiple groups.

Results

Identification of cells in microtia

A freshly isolated single-cell suspension from human auricular cartilage was obtained through uniform sampling (Fig. 1A), followed by enzymatic digestion and density gradient centrifugation. Prior to further analysis, we performed quality control of the raw data and excluded cells with low data quality. Thereafter, 45,875 total cells were obtained for subsequent analysis. The UMAP algorithm clustered cells into 15 groups, which were then annotated as known cell types (chondrocytes, stromal cells, endothelial cells, stem cells, and immune cells) using standard cell markers (Fig. 1B,C). Figure 1D,E show the composition and changes of each cell in normal and microtia. Compared to the normal group, the proportion of chondrocytes is decreased in the microtia group. Our HE and Safranin-O-fast green staining results suggest that there is a gradual transition process between the perichondrium and cartilage in normal ear cartilage (Fig. 1F). Near the perichondrium, chondrocytes are smaller, flattened, and distributed individually, with the surrounding matrix showing acidophilic red staining. In the deeper layers, chondrocytes are larger, with more isogenous cell groups, and numerous bundle-like elastic fibers can be faintly seen in the matrix. In microtia cartilage, the perichondrium is thicker, and the transition between the perichondrium and chondrocytes is less distinct. There are more immature chondrocytes, with a larger area of light red staining in the matrix. In the deeper layers, there are fewer isogenous cell groups, and coarse fibers exist between the cells. We performed fine-resolution clustering and annotation and applied the miloR tool to quantify shifts in the abundance of all cell types between groups (Fig. 1G). The analysis revealed significant differences in cellular composition between microtia cartilage and normal auricular cartilage samples.

Heterogeneity between cell clusters of chondrocytes

Mitochondrial function score suggested that mitochondrial score in microtia chondrocytes was lower than that in normal ear chondrocytes (Figs. 2A). Figure 2B shows the UMAP visualization of single-cell transcriptomes from normal control and microtia samples, with cells clustered and annotated into distinct populations including chondrocytes, immune cells, stem cells, and endothelial cells. The color intensity represents mitochondrial function scores, where brighter colors indicate higher scores and darker colors indicate lower scores. In the visualization, chondrocytes from microtia samples displayed notably darker coloring compared to those from normal controls, indicating lower mitochondrial scores. This difference in mitochondrial scores between normal and microtia chondrocytes suggests altered mitochondrial function in the diseased state, which may contribute to the pathogenesis of microtia. We compared the difference in the proportion of cell types in the microtia and normal groups using UMAP diagrams. We further dissected the chondrocytes subpopulation and showed that not all chondrocytes were universally deregulated, cluster 0,1,4,5,6,10 demonstrating a significant increase (Fig. 2C).

In Fig. 2D, UMAP visualization reveals distinct mitochondrial function patterns between normal and microtia chondrocytes, where color intensity represents mitochondrial function scores (brighter colors indicating higher scores, darker colors indicating lower scores). The normal ear chondrocytes predominantly display a brighter color, while microtia chondrocytes exhibit a notably darker color, suggesting reduced mitochondrial function scores in microtia samples compared to normal controls. Mitochondrial scores of clusters 3 and 7 were higher than those of other clusters. We defined chondrocytes with higher than average mitochondrial scores as having high mitochondrial function (increase_chon) and chondrocytes with lower than average mitochondrial function (decrease_chon). The cell–cell communication analysis was performed using the cellchat pipeline. In detail, the frequency and intensity of interactions between increase_chon and stromal cell, between decrease_chon and stromal cell were high (Fig. 2E). Figure 2F shows that increase_chon exhibit enhanced input interaction strength than decrease_chon. Moreover, increase_chon received more signals mediated by TGF-β, OSM, BMP, and VISFATIN, while decrease_chon sent more signals to other cells mediated by MIF, SEMA3, and BMP, and received more signals mediated by HGF, TGF-β, OSM, and MK (Fig. 2G). We then analyzed and compared the specific pathways by which various cell types exhibit stronger interactions (Fig. 2H,I), the results showed that stromal cell sent stronger signals to increase_chon in the BMP-related pathway and IGF-related pathway compared to decrease_chon, and increase_chon sent stronger signals to stromal cell in the GAS6-related pathway compared to decrease_chon (Fig. 2H-I). Based on the Fig. 3A,B, we can observe distinct differences in the developmental trajectories of normal ear cartilage and microtia ear cartilage. In the case of normal ear cartilage, two primary differentiation paths are evident, with the main trajectory oriented towards regions of higher mitochondrial scores (Fig. 3A). This suggests a more organized and directed developmental process in normal chondrocytes. In contrast, the microtia ear cartilage exhibits a more complex pattern with three discernible differentiation

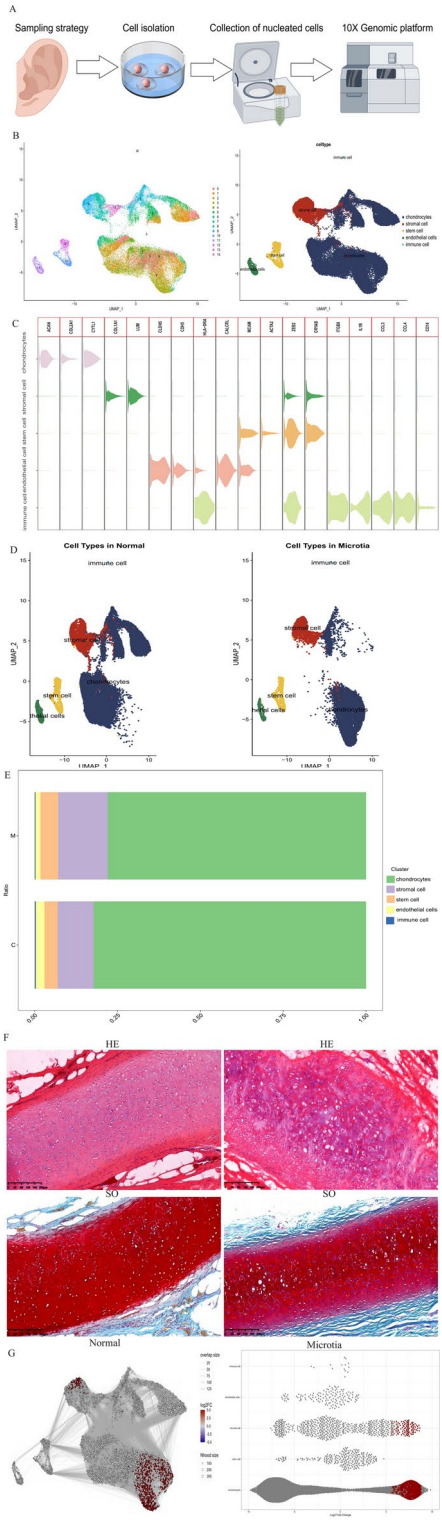

Fig. 1. Analysis of single-cell RNA sequencing. (**A**) Schematic diagram of the experimental design. (**B**) UMAP plot showing cell clusters identified in microtia and normal ear cartilage samples. (**C**) Dot plot showing representative marker genes for each cell type. (**D**) The cell types are identified by marker genes. (**E**) Differential abundance of cell types between normal and microtia samples. (**F**) H&E and Safranin O-Fast Green staining of normal and microtia ear cartilage sections. (**G**) Neighborhood graph using Milo differential abundance testing. Nodes represent neighborhoods from the cell population. Colors indicate the log2-fold difference between patients with microtia and healthy group. Neighborhoods that increased in patients with microtia are shown in red. Neighborhoods decreased in patients with microtia are shown in blue.

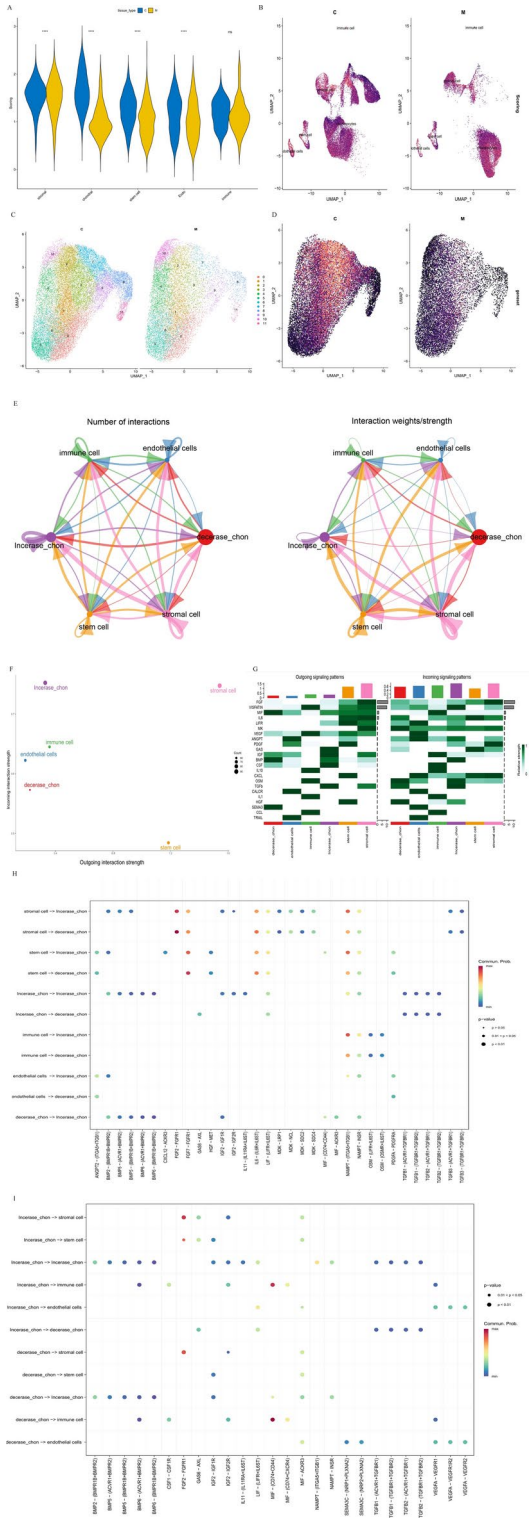

Fig. 2. Heterogeneity and cell–cell communication analysis of chondrocyte clusters. (**A**) Comparison of mitochondrial function scores between normal and microtia chondrocytes. (**B**) UMAP plot showing mitochondrial function scores in chondrocytes. (**C**) UMAP plots showing differential abundance of chondrocyte clusters between normal and microtia samples. (**D**) Mitochondrial function scores across different chondrocyte clusters. The color intensity corresponds to the mitochondrial score, with brighter colors indicating higher scores. (**E**) Strength and number of interactions between key cells, where the width of each connecting line represents the strength of cellular interactions, and different colors indicate distinct signaling pathways. (**F**) The cell communication network is visualized in terms of signal communication. (**G**) Interaction quantity and interaction weight/strength of various cells in the communication network. (**H**,**I**) Bubble plots show specific pathways by which different cell types exhibit stronger interactions.

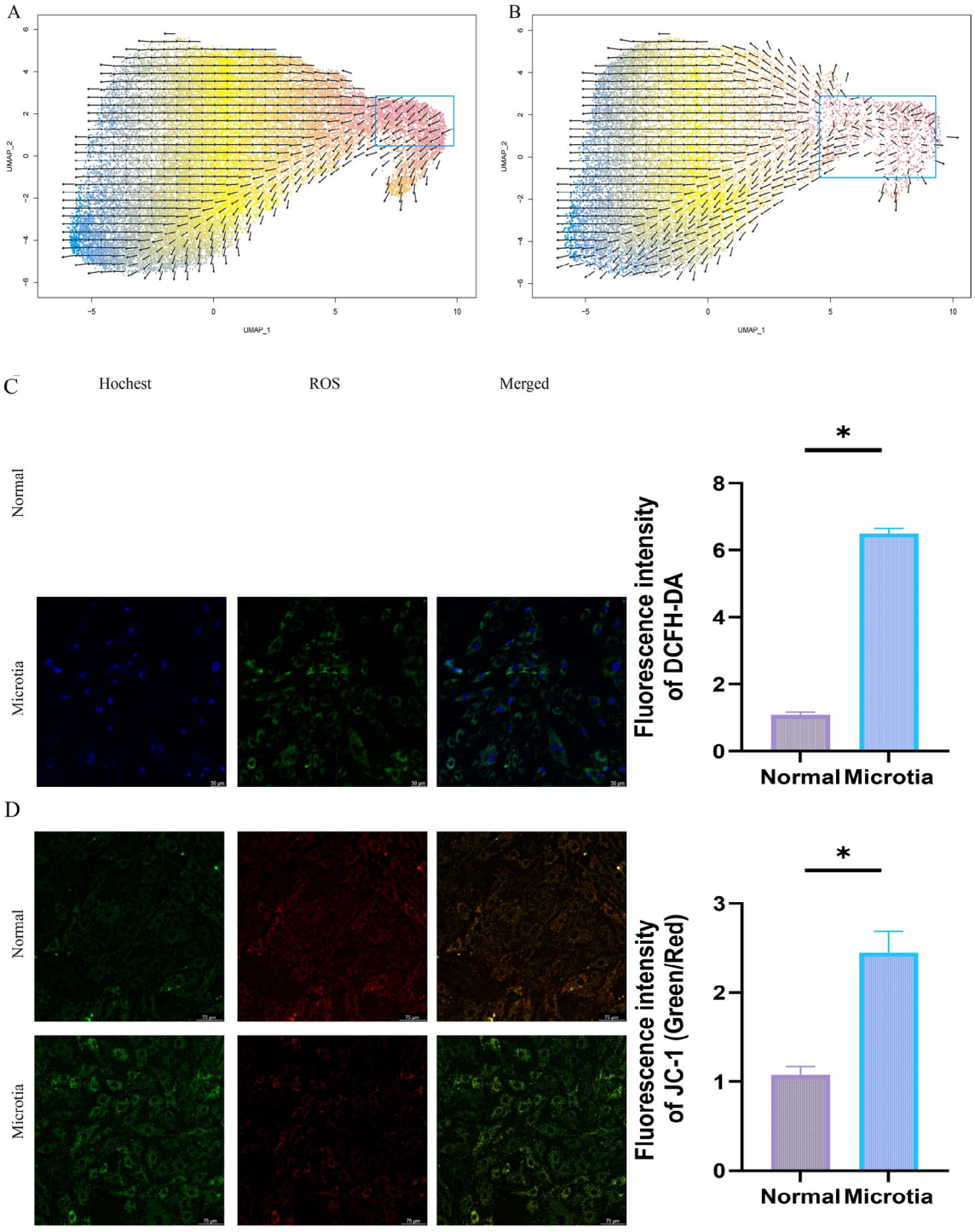

Fig. 3. (**A**,**B**) UMAP plot showing the inferred developmental trajectory of chondrocytes, where colors in the RNA velocity plot represent pseudotime progression of chondrocyte differentiation, with red indicating earlier developmental stages (start of trajectory), yellow representing intermediate stages, and blue indicating later developmental stages (end of trajectory). (**C**) Intracellular ROS levels in normal and microtia chondrocytes. Left panels: Fluorescence microscopy images showing Hoechst nuclear staining (blue), ROS levels detected by DCFH-DA (green), and merged images. Scale bar = 50 μm. Right panel: Quantification of DCFH-DA fluorescence intensity in normal and microtia chondrocytes. *$p < 0.05$." (**D**) Mitochondrial membrane potential in normal and microtia chondrocytes. The left panels show fluorescence microscopy images of mitochondrial membrane potential measured by JC-1 staining, where green fluorescence indicates monomeric form (low membrane potential), red fluorescence shows aggregated form (high membrane potential), and merged images display the combination of both signals. The right panel presents the quantitative analysis comparing the ratio of green to red fluorescence intensity (JC-1 monomer/aggregate ratio) between normal and microtia chondrocytes, with a higher ratio indicating lower mitochondrial membrane potential. *$p < 0.05$.

trajectories. Notably, compared to the normal ear cartilage, the differentiation directions in microtia appear more disorganized and chaotic. This increased complexity and apparent disorder in the microtia sample may indicate alterations in the normal developmental processes of chondrocytes, potentially contributing to the malformation observed in microtia. The divergence in trajectory patterns between normal and microtia samples highlights the dysregulation of chondrocyte differentiation in the pathological condition.

Mitochondrial dysfunction in microtia chondrocytes

Mitochondrial ROS results are shown in Fig. 3C. Chondrocytes from microtia produce significantly higher levels of ROS compared to normal auricular chondrocytes ($P < 0.05$). Mitochondrial membrane potentials were analyzed by the use of a dual-wavelength fluorescent probe, JC-1, which as a monomer emits green fluorescence and in a reaction driven by the mitochondrial membrane potential converts to a red-fluorescence–emitting dimer. As seen in Fig. 3D, the ratio of green/red JC-1 fluorescence was significantly lower in normal auricular chondrocytes relative to the chondrocytes from microtia ($P < 0.05$), suggesting functional mitochondrial alterations.

HdWGCNA identifies hub genes associated with mitochondrial dysfunction in chondrocytes

To investigate the intrinsic functions and properties of chondrocytes with high mitochondrial scores, we constructed a co-expression network based on single-cell data using an optimal soft threshold of 12, as illustrated in Fig. 4A. Figure 4B shows the hierarchical clustering dendrogram of the co-expression network, where each short vertical line represents an individual gene. Genes with similar expression patterns are clustered together in branches, with the height of branches indicating the dissimilarity between clusters. The dendrogram identified 15 distinct gene modules, represented by different colors at the bottom, where genes within the same colored module share highly correlated expression patterns. Figure 4C presents the top 10 hub genes for these 15 modules, where each colored shape shows the distribution of kME (eigengene-based connectivity) values within a module. The kME values, shown on the y-axis, represent each gene's connectivity within its module, with higher values indicating stronger potential hub genes. For each module, genes are ordered by increasing kME values, with the top 10 highest-connectivity genes labeled. Genes highlighted in yellow and cyan within the gene modules exhibited a higher likelihood of expression in clusters 3 and 7, respectively, demonstrating a significant positive correlation (Fig. 4D). In addition, the red module shows a strong positive correlation in the brown module, the blue module shows a strong positive correlation with the pink and tan module, and the yellow module has a strong positive correlation with the salmon module (Fig. 4E). We then scored the genes of the top 25 hub genes ranked by kME in each module (Fig. 4F).

Pseudo-time and trajectory analysis

To determine the transcriptional characteristics of chondrocytes at different stages of development, we performed a pseudo-temporal analysis. Cells that have similar states are grouped, and branch points divide cells into different states. We constructed a pseudotime developmental tree and determined five independent branch points (Fig. 5A). The 12 chondrocytes subclusters scattered at different branches in the developmental tree (Fig. 5B). Clusters 3 and 7 were predominantly distributed in the early stages of the developmental trajectory, suggesting they represent earlier developmental stages compared to other subclusters. To further investigate the genes in the clusters 3 and 7, we conducted a pseudotime analysis on the hub genes within these clusters. Our findings revealed that these genes were expressed earliest in the pseudotemporal trajectory, marking the initiation of the developmental process (Fig. 5C).

The genes in the yellow and cyan modules was analyzed for functional enrichment

The function of genes in the yellow and cyan modules was investigated by conducting an enrichment analysis on the top 25 hub genes within these modules, resulting in a total of 50 genes in the yellow and cyan modules. The GO analysis revealed that hub genes were significantly enriched in processes related to metabolic process, response to endoplasmic reticulum stress, mitochondrial matrix, and electron transfer activity (Fig. S1A-C) and KEGG analysis displayed that "Oxidative phosphorylation", "Protein export", and "Antigen processing and presentation" pathways depicted predominant enrichment of genes (Fig. S1D)[19]. Figure 6A shows the results of the friends analysis of these hub genes. The results showed that the six genes with the strongest correlation were SDHA, SIRT1, HNRNPF, PGC1A, UBE2D3 and CYCS. We performed PPI analysis of hub genes through the STRING database and visualized and mapped the results of protein interactions, 45 genes were found to have strong biological functional similarities (Fig. 6B). Next, we drew violin plots showing how much of the top 6 hub genes was expressed (Fig. 6C). In chondrocytes of microtia, the expression of SDHA, SIRT1, and PGC1A is reduced compared to normal auricular chondrocytes (Fig. 6C). Our Western blot results also confirm this finding (Fig. 6D).

Discussion

This study provides novel and comprehensive insights into the cellular and molecular mechanisms underlying microtia by demonstrating significant mitochondrial dysfunction in chondrocytes from microtia patients. Our single-cell RNA sequencing analysis revealed lower mitochondrial function scores in microtia chondrocytes compared to normal samples, suggesting impaired mitochondrial activity. This finding was further corroborated by increased ROS production, decreased mitochondrial membrane potential, and altered mitochondrial structure observed in microtia chondrocytes. These results collectively point to a critical role of mitochondrial dysfunction in the pathogenesis of microtia, offering a new perspective on this congenital malformation.

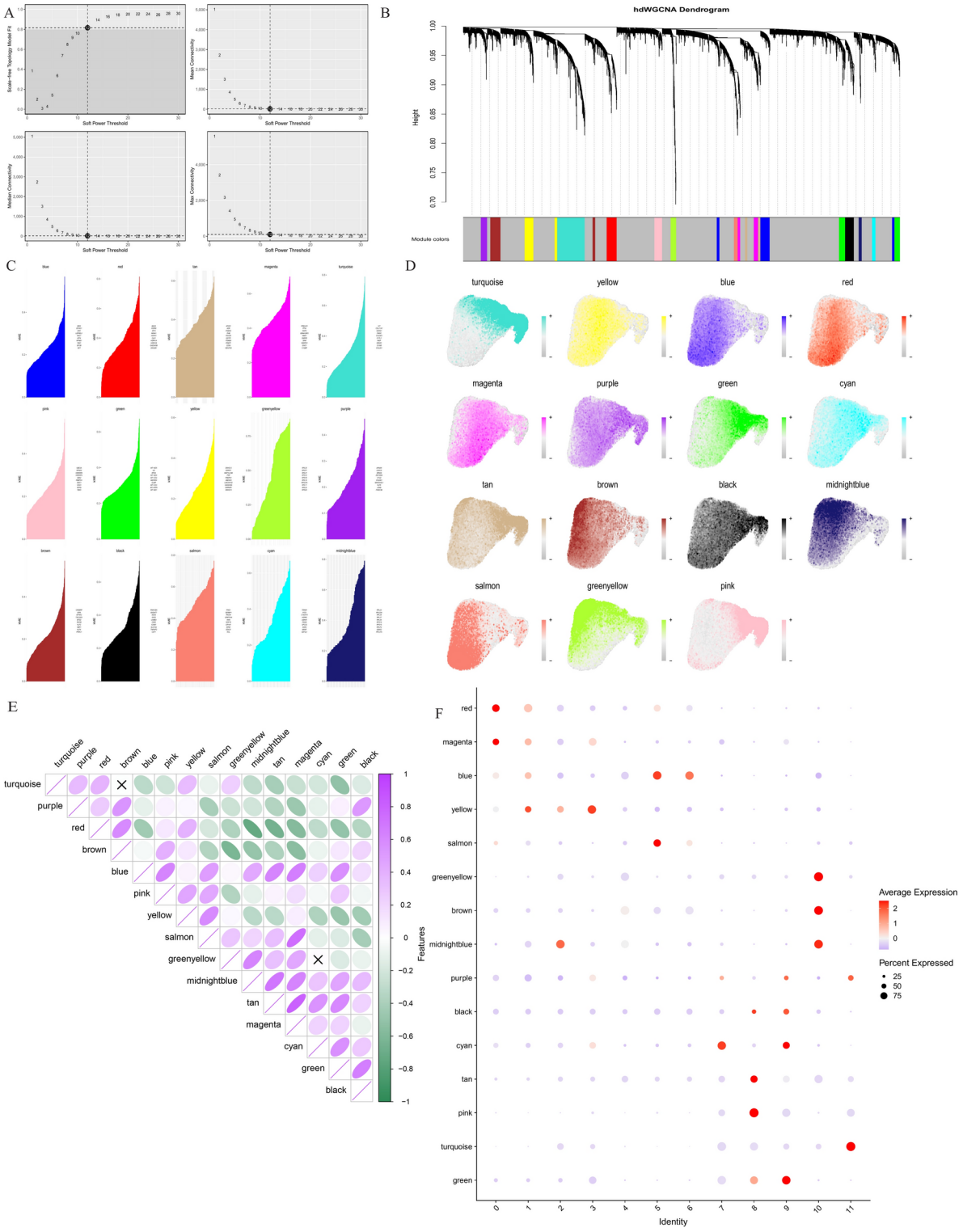

Fig. 4. (**A**) Select a soft power supply suitable for running the hdWGCNA, the mean value, median value and maximum connectivity of the topology network are shown respectively when different minimum soft thresholds are selected. (**B**) 15 modules are identified as shown in the tree diagram. (**C**) Each module presents the top hub gene. (**D**) The feather plot depicts the score for 15 modules. (**E**) Correlation analysis between different models. This correlation matrix shows the relationships between different gene modules, where the color and shape of ellipses represent the strength and direction of correlations. Purple indicates positive correlations while green indicates negative correlations, with darker colors showing stronger correlations. The correlation coefficients range from -1 to + 1, where more elongated ellipses indicate stronger relationships between modules. (**F**) Bubble plot reveals the scores obtained by each module.

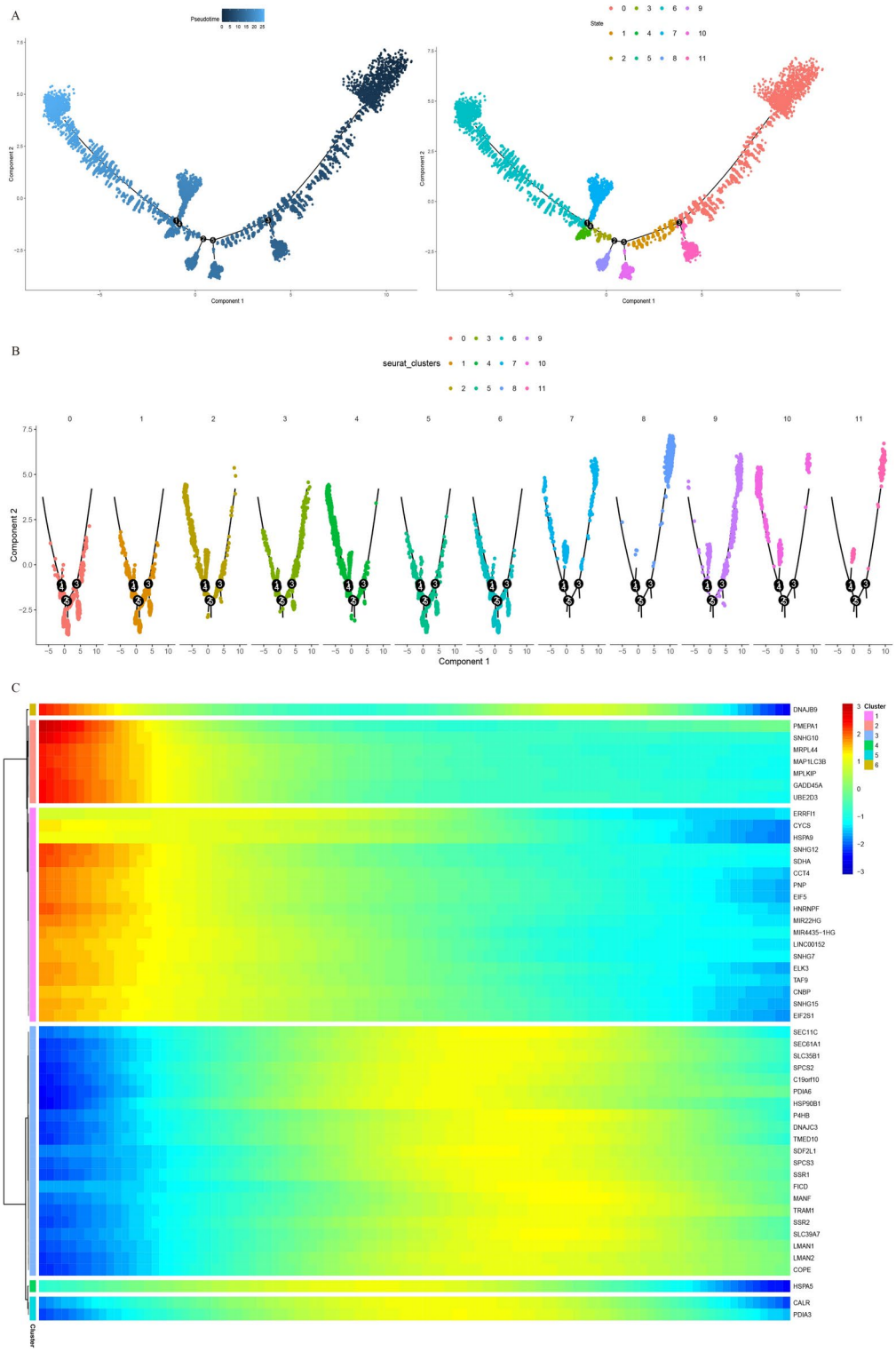

Fig. 5. (**A**) Pseudotime distribution of the different chondrocytes subtypes. (**B**) Pseudotime distribution of the different chondrocytes clusters. (**C**) Heat maps showed the expression of genes in chondrocytes clusters 3 and 7. The colors in this heatmap represent gene expression levels along the pseudotime trajectory, where red indicates high expression, yellow indicates intermediate expression, and blue indicates low expression. The 6 clusters shown in the legend are automatically generated by the trajectory analysis algorithm and are distinct from our previous cell clustering results. These clusters represent different states along the continuous developmental trajectory, as shown on the x-axis, which displays the pseudotime progression from left to right.

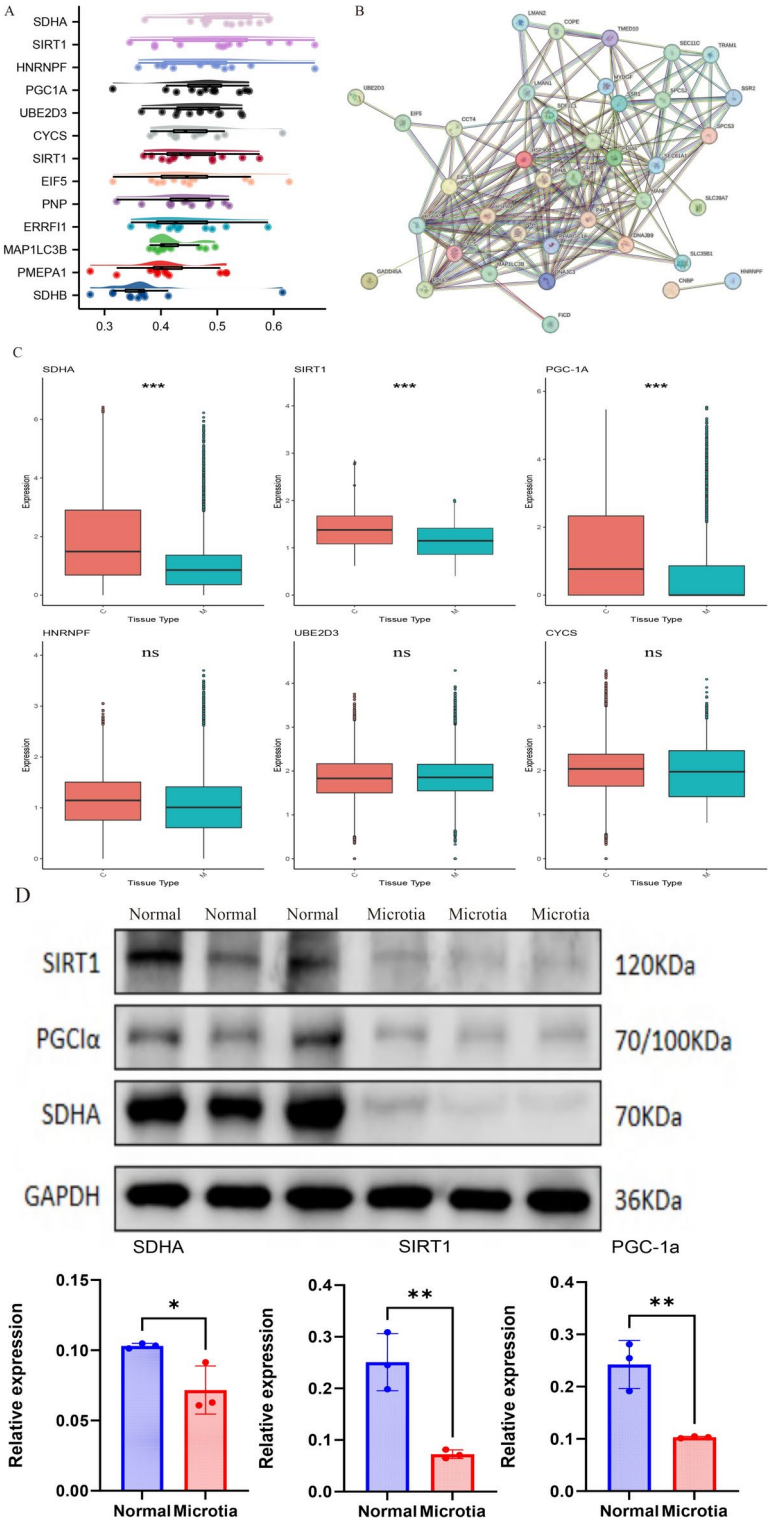

Fig. 6. (**A**) Friends analysis of genes in the yellow and cyan modules, the total score ranges from 0 to 1, with higher scores indicating more genes associated with it. (**B**) PPI of genes in the yellow and cyan modules. (**C**) The expression differences of SDHA, SIRT1, and PGC1A between normal and microtia ear cartilage.*$p < 0.05$.**$p < 0.01$.***$p < 0.001$. (**D**) Western blot analysis of SDHA, SIRT1, and PGC1A protein levels in normal and microtia ear cartilage.*$p < 0.05$.**$p < 0.01$.

Mitochondrial dysfunction in microtia chondrocytes

The observation of mitochondrial dysfunction in microtia chondrocytes is a key finding of our study. Mitochondria play crucial roles in cellular energy production, redox balance, and various signaling pathways[20,21]. The impaired mitochondrial function we observed could have far-reaching consequences on chondrocyte metabolism, proliferation, differentiation, and ultimately, on the development and maintenance of auricular cartilage. The increased ROS production in microtia chondrocytes is particularly noteworthy. While low levels of ROS are important for cellular signaling, excessive ROS can lead to oxidative stress, causing damage to cellular components including proteins, lipids, and DNA[22]. In the context of chondrocytes, elevated ROS levels have been associated with impaired extracellular matrix synthesis, increased matrix degradation, and induction of cellular senescence[23,24]. These effects could contribute to the abnormal cartilage formation and growth observed in microtia. The decreased mitochondrial membrane potential in microtia chondrocytes further supports the presence of mitochondrial dysfunction. Mitochondrial membrane potential is crucial for ATP production through oxidative phosphorylation[25]. A reduction in membrane potential could lead to decreased ATP production, potentially compromising energy-dependent processes essential for proper chondrocyte function and cartilage development. The alterations in mitochondrial structure observed through transmission electron microscopy provide additional evidence of mitochondrial abnormalities in microtia chondrocytes. Changes in mitochondrial morphology have been linked to various aspects of mitochondrial function, including energy production, apoptosis regulation, and calcium homeostasis[26]. A key finding of our study is the heterogeneity among chondrocyte subpopulations in microtia samples. Not all chondrocytes were uniformly affected, with certain clusters showing significant alterations in proportion and mitochondrial function. This heterogeneity may explain the variable clinical presentations of microtia and highlights the complexity of the disease mechanism. The observed differences in cell–cell communication patterns between chondrocytes with high and low mitochondrial function scores provide further evidence for the functional implications of this heterogeneity. Intercellular communication is crucial for coordinating tissue development and homeostasis[27]. Altered communication patterns could disrupt the delicate balance of signaling molecules necessary for proper cartilage formation and maintenance. This heterogeneity also raises important questions about the origins and progression of mitochondrial dysfunction in microtia. It is possible that the observed heterogeneity reflects different stages of disease progression, with some chondrocytes more severely affected than others. Alternatively, it could indicate the existence of distinct subpopulations of chondrocytes with varying susceptibilities to mitochondrial dysfunction. Future studies employing lineage tracing techniques could help elucidate the developmental origins of these heterogeneous populations and their roles in microtia pathogenesis.

Gene co-expression network analysis and hub genes

Our gene co-expression network analysis identified several hub genes associated with mitochondrial function, including SDHA, SIRT1, and PGC1A, which showed reduced expression in microtia chondrocytes. These findings provide valuable insights into the molecular mechanisms underlying mitochondrial dysfunction in microtia.

SDHA (Succinate Dehydrogenase Complex Flavoprotein Subunit A) is a key component of both the mitochondrial respiratory chain complex II and the tricarboxylic acid (TCA) cycle[28]. Its reduced expression in microtia chondrocytes could directly impact energy production through both oxidative phosphorylation and the TCA cycle. This could lead to a metabolic shift in chondrocytes, potentially affecting their ability to produce and maintain cartilage extracellular matrix. Moreover, mutations in SDHA have been associated with various mitochondrial disorders[29], suggesting that its downregulation could have broad implications for mitochondrial function.

SIRT1 (Sirtuin 1) is a NAD + -dependent deacetylase that plays crucial roles in cellular metabolism, stress responses, and aging[30]. In the context of mitochondrial function, SIRT1 has been shown to regulate mitochondrial biogenesis and function through deacetylation of PGC1A and other targets[31]. The reduced expression of SIRT1 in microtia chondrocytes could lead to impaired mitochondrial biogenesis and function, contributing to the observed mitochondrial dysfunction.

PGC1A (Peroxisome Proliferator-Activated Receptor Gamma Coactivator 1-Alpha) is a master regulator of mitochondrial biogenesis and function[32]. Its downregulation in microtia chondrocytes suggests a potential mechanism for the observed mitochondrial dysfunction. PGC1A coordinates the expression of numerous genes involved in mitochondrial metabolism, including those encoding respiratory chain components and antioxidant enzymes[33]. Reduced PGC1A expression could lead to decreased mitochondrial content and impaired antioxidant defenses, consistent with our observations of mitochondrial dysfunction and increased ROS production.

Our findings regarding mitochondrial dysfunction in microtia chondrocytes are consistent with recent studies in related cartilage disorders. Previous studies have demonstrated that mitochondrial dysfunction in chondrocytes leads to disrupted cellular differentiation and accelerated cartilage degradation through increased oxidative stress and inflammatory responses[34]. The mitochondrial dysfunction observed in microtia chondrocytes could be attributed to multiple factors, including genetic mutations affecting mitochondrial DNA or nuclear genes encoding mitochondrial proteins, environmental stressors during early embryonic development, and dysregulation of key mitochondrial quality control pathways. The identification of these hub genes not only provides mechanistic insights into mitochondrial dysfunction in microtia but also suggests potential therapeutic targets. Strategies aimed at upregulating or activating these genes could potentially ameliorate mitochondrial dysfunction and improve chondrocyte function in microtia patients.

Altered chondrocyte trajectory and differentiation patterns

The altered trajectory and more disorganized differentiation patterns observed in microtia chondrocytes point to a developmental aspect of the disease. This finding aligns with the congenital nature of microtia and suggests

that mitochondrial dysfunction may play a role in the abnormal development of auricular cartilage. During normal cartilage development, chondrocytes undergo a tightly regulated process of proliferation, differentiation, and maturation. Our trajectory analysis suggests that this process is disrupted in microtia, potentially due to mitochondrial dysfunction. The more disorganized differentiation patterns observed in microtia chondrocytes could lead to abnormal cartilage structure and function.

The link between mitochondrial function and chondrocyte differentiation is supported by several lines of evidence. Mitochondrial metabolism has been shown to play a crucial role in stem cell differentiation and fate decisions[35]. In the context of chondrogenesis, shifts in metabolic profiles have been observed during different stages of chondrocyte differentiation. The mitochondrial dysfunction we observed in microtia chondrocytes could disrupt these metabolic shifts, leading to abnormal differentiation patterns. Moreover, ROS, which we found to be elevated in microtia chondrocytes, have been implicated in the regulation of chondrocyte differentiation. While low levels of ROS can act as signaling molecules promoting differentiation, excessive ROS can impair chondrogenesis and lead to premature senescence of chondrocytes[36]. The increased ROS production in microtia chondrocytes could thus contribute to the altered differentiation patterns we observed. The disrupted balance between chondrocyte proliferation and differentiation, potentially due to mitochondrial dysfunction, could contribute to the malformation of the external ear. This suggests that interventions aimed at restoring normal mitochondrial function and redox balance could potentially normalize chondrocyte differentiation and improve auricular cartilage development in microtia patients.

Our histological and ultrastructural analyses provide further evidence for the cellular and tissue-level changes in microtia. The thicker perichondrium, less distinct transition between perichondrium and chondrocytes, and altered matrix composition in microtia samples suggest widespread changes in tissue organization and extracellular matrix production. These changes may be secondary to the mitochondrial dysfunction observed at the cellular level. The thicker perichondrium observed in microtia samples could reflect an adaptive response to impaired cartilage formation. The perichondrium plays crucial roles in cartilage growth and repair, serving as a source of chondrocyte progenitors and regulating cartilage homeostasis. The thickening of this layer might represent an attempt to compensate for deficient cartilage formation or maintenance due to dysfunctional chondrocytes. The less distinct transition between perichondrium and chondrocytes in microtia samples is particularly intriguing. This observation suggests a potential disruption in the normal differentiation of perichondrial cells into chondrocytes, which is a crucial process in cartilage growth. This finding aligns with our trajectory analysis results, further supporting the notion of altered chondrocyte differentiation in microtia.

The changes in extracellular matrix composition observed in microtia samples, including altered proteoglycan distribution and collagen organization, could have significant implications for cartilage function. The extracellular matrix is crucial for maintaining the structural and functional properties of cartilage. Alterations in matrix composition could affect the mechanical properties of the tissue, potentially contributing to the abnormal shape and structure of the external ear in microtia. These histological and ultrastructural changes could be directly linked to the mitochondrial dysfunction we observed in microtia chondrocytes. Mitochondrial function is crucial for the energy-demanding processes of matrix synthesis and remodeling[37]. Impaired mitochondrial function could lead to reduced production of matrix components and altered matrix organization. Moreover, the increased ROS production associated with mitochondrial dysfunction could contribute to matrix degradation through oxidative damage and activation of matrix-degrading enzymes[38].

Implications for microtia pathogenesis and potential therapeutic approaches

Strategies to improve mitochondrial function offer promising interventions for microtia. Mitochondrial-targeted antioxidants like MitoQ could reduce oxidative stress and improve mitochondrial function in microtia chondrocytes. Activators of mitochondrial biogenesis, such as AMPK or SIRT1 activators, could increase mitochondrial content and function. Metabolic modulation strategies, including alternative energy substrates or pathway modulation, may compensate for impaired mitochondrial function. Gene therapy targeting SDHA, SIRT1, and PGC1A could potentially restore mitochondrial function in affected chondrocytes. Cell-based therapies involving isolation and expansion of chondrocytes with higher mitochondrial function might be beneficial. Incorporating mitochondrial function enhancement into existing tissue engineering approaches for auricular reconstruction could improve outcomes.

Conclusion

In conclusion, our study provides compelling evidence for mitochondrial dysfunction in microtia chondrocytes and identifies potential key genes involved in this process. These findings not only advance our understanding of the pathogenesis of microtia but also pave the way for the development of novel therapeutic strategies. The observed mitochondrial dysfunction appears to be intricately linked to various cellular and tissue-level abnormalities in microtia, including altered chondrocyte differentiation, abnormal matrix production, and tissue structural changes.

The heterogeneity among chondrocyte populations and the identification of specific hub genes associated with mitochondrial function provide valuable insights into the complexity of microtia pathogenesis and suggest potential targets for therapeutic intervention. Our findings open up new avenues for treatment, including mitochondrial-targeted therapies, metabolic modulation, and gene therapy approaches.

While significant work remains to be done to fully elucidate the role of mitochondrial dysfunction in microtia and to translate these findings into clinical applications, our study represents a significant step forward in understanding this complex condition. Future studies building on these findings have the potential to dramatically improve our ability to diagnose, treat, and potentially prevent microtia, offering hope to affected individuals and their families.

Data availability

Data set can be made available upon request to the corresponding author.

Received: 8 October 2024; Accepted: 1 January 2025
Published online: 06 January 2025

References

1. Li, X. et al. The congenital birth defects burden in children younger than 14 years of age, 1990–2019: An age-period-cohort analysis of the global burden of disease study. *J. Glob. Health* **14**, 4012. https://doi.org/10.7189/jogh.14.04012 (2024).
2. Hou, R. et al. Prussian blue nanozyme promotes the survival rate of skin flaps by maintaining a normal microenvironment. *ACS Nano* **16**, 9559–9571. https://doi.org/10.1021/acsnano.2c02832 (2022).
3. Luquetti, D. V., Heike, C. L., Hing, A. V., Cunningham, M. L. & Cox, T. C. Microtia: Epidemiology and genetics. *Am. J. Med. Genet. A* **158A**, 124–139. https://doi.org/10.1002/ajmg.a.34352 (2012).
4. Liu, X., Zheng, C., Gao, X., Chen, J. & Zheng, K. Complete molecular and immunoprotective characterization of babesia microti enolase. *Front. Microbiol.* **8**, 622. https://doi.org/10.3389/fmicb.2017.00622 (2017).
5. Bader, V. & Winklhofer, K. F. Mitochondria at the interface between neurodegeneration and neuroinflammation. *Semin. Cell Dev. Biol.* **99**, 163–171. https://doi.org/10.1016/j.semcdb.2019.05.028 (2020).
6. Faas, M. M. & de Vos, P. Mitochondrial function in immune cells in health and disease. *Biochim. Biophys. Acta* **1866**, 165845. https://doi.org/10.1016/j.bbadis.2020.165845 (2020).
7. Riley, J. S. & Tait, S. W. Mitochondrial DNA in inflammation and immunity. *EMBO Rep.* **21**, e49799. https://doi.org/10.15252/embr.201949799 (2020).
8. Nunnari, J. & Suomalainen, A. Mitochondria: In sickness and in health. *Cell* **148**, 1145–1159. https://doi.org/10.1016/j.cell.2012.02.035 (2012).
9. Gorman, G. S. et al. Mitochondrial diseases. *Nat. Rev. Dis. Primers* **2**, 16080. https://doi.org/10.1038/nrdp.2016.80 (2016).
10. Khacho, M. & Slack, R. S. Mitochondrial activity in the regulation of stem cell self-renewal and differentiation. *Curr. Opin. Cell Biol.* **49**, 1–8. https://doi.org/10.1016/j.ceb.2017.11.003 (2017).
11. Rojo, A. I. et al. Redox control of microglial function: Molecular mechanisms and functional significance. *Antioxid. Redox Signal.* **21**, 1766–1801. https://doi.org/10.1089/ars.2013.5745 (2014).
12. Chiurazzi, M., Di Maro, M., Cozzolino, M. & Colantuoni, A. Mitochondrial dynamics and microglia as new targets in metabolism regulation. *Int. J. Mol. Sci.* https://doi.org/10.3390/ijms21103450 (2020).
13. Agrawal, I. & Jha, S. Mitochondrial dysfunction and Alzheimer's disease: Role of microglia. *Front. Aging Neurosci.* **12**, 252. https://doi.org/10.3389/fnagi.2020.00252 (2020).
14. Rath, S. et al. MitoCarta3.0: An updated mitochondrial proteome now with sub-organelle localization and pathway annotations. *Nucleic Acids Res.* **49**, D1541–D1547. https://doi.org/10.1093/nar/gkaa1011 (2021).
15. Langfelder, P. & Horvath, S. WGCNA: An R package for weighted correlation network analysis. *Bmc Bioinform.* **9**, 559. https://doi.org/10.1186/1471-2105-9-559 (2008).
16. Zhang, F., Li, X. & Tian, W. Unsupervised inference of developmental directions for single cells using VECTOR. *Cell Rep.* **32**, 108069. https://doi.org/10.1016/j.celrep.2020.108069 (2020).
17. Lyublinskaya, O. G. et al. Redox environment in stem and differentiated cells: A quantitative approach. *Redox Biol.* **12**, 758–769. https://doi.org/10.1016/j.redox.2017.04.016 (2017).
18. Horwath, M. C. et al. Antifungal activity of the lipophilic antioxidant ferrostatin-1. *Chembiochem* **18**, 2069–2078. https://doi.org/10.1002/cbic.201700105 (2017).
19. Kanehisa, M. & Goto, S. KEGG: Kyoto encyclopedia of genes and genomes. *Nucleic Acids Res.* **28**, 27–30 (2000).
20. Liu, L. et al. Urea transport B gene induces melanoma B16 cell death via activation of p53 and mitochondrial apoptosis. *Cancer Sci.* **109**, 3762–3773. https://doi.org/10.1111/cas.13825 (2018).
21. Ma, Y. et al. Immature rat testis sustained long-term development using an integrative model. *Biol. Res.* **55**, 30. https://doi.org/10.1186/s40659-022-00398-y (2022).
22. Murphy, M. P. How mitochondria produce reactive oxygen species. *Biochem. J.* **417**, 1–13. https://doi.org/10.1042/BJ20081386 (2009).
23. Lepetsos, P. & Papavassiliou, A. G. ROS/oxidative stress signaling in osteoarthritis. *Biochim. Biophys. Acta* **1862**, 576–591. https://doi.org/10.1016/j.bbadis.2016.01.003 (2016).
24. Loeser, R. F., Collins, J. A. & Diekman, B. O. Ageing and the pathogenesis of osteoarthritis. *Nat. Rev. Rheumatol.* **12**, 412–420. https://doi.org/10.1038/nrrheum.2016.65 (2016).
25. Ding, N. et al. AGK regulates the progression to NASH by affecting mitochondria complex I function. *Theranostics* **12**, 3237–3250. https://doi.org/10.7150/thno.69826 (2022).
26. Picard, M., McEwen, B. S., Epel, E. S. & Sandi, C. An energetic view of stress: Focus on mitochondria. *Front. Neuroendocrinol.* **49**, 72–85. https://doi.org/10.1016/j.yfrne.2018.01.001 (2018).
27. Su, J. et al. Cell-cell communication: New insights and clinical implications. *Signal Transduct. Target. Ther.* **9**, 196. https://doi.org/10.1038/s41392-024-01888-z (2024).
28. Huang, Y. et al. Germline SDHB and SDHD mutations in pheochromocytoma and paraganglioma patients. *Endocr. Connect.* **7**, 1217–1225. https://doi.org/10.1530/EC-18-0325 (2018).
29. Renkema, G. H. et al. SDHA mutations causing a multisystem mitochondrial disease: Novel mutations and genetic overlap with hereditary tumors. *Eur. J. Hum. Genet. Ejhg* **23**, 202–209. https://doi.org/10.1038/ejhg.2014.80 (2015).
30. Cantó, C. & Auwerx, J. PGC-1alpha, SIRT1 and AMPK, an energy sensing network that controls energy expenditure. *Curr. Opin. Lipidol.* **20**, 98–105. https://doi.org/10.1097/MOL.0b013e328328d0a4 (2009).
31. Rodgers, J. T. et al. Nutrient control of glucose homeostasis through a complex of PGC-1alpha and SIRT1. *Nature* **434**, 113–118 (2005).
32. Fernandez-Marcos, P. J. & Auwerx, J. Regulation of PGC-1α, a nodal regulator of mitochondrial biogenesis. *Am. J. Clin. Nutr.* **93**, 884S-890S. https://doi.org/10.3945/ajcn.110.001917 (2011).
33. Austin, S. & St-Pierre, J. PGC1α and mitochondrial metabolism–emerging concepts and relevance in ageing and neurodegenerative disorders. *J. Cell Sci.* **125**, 4963–4971. https://doi.org/10.1242/jcs.113662 (2012).
34. Jiang, W. et al. Mechanisms linking mitochondrial mechanotransduction and chondrocyte biology in the pathogenesis of osteoarthritis. *Ageing Res. Rev.* **67**, 101315. https://doi.org/10.1016/j.arr.2021.101315 (2021).
35. Folmes, C. D. L., Dzeja, P. P., Nelson, T. J. & Terzic, A. Metabolic plasticity in stem cell homeostasis and differentiation. *Cell Stem Cell* **11**, 596–606. https://doi.org/10.1016/j.stem.2012.10.002 (2012).
36. Morita, K. et al. Reactive oxygen species induce chondrocyte hypertrophy in endochondral ossification. *J. Exp. Med.* **204**, 1613–1623 (2007).
37. Blanco, F. J., Rego, I. & Ruiz-Romero, C. The role of mitochondria in osteoarthritis. *Nat. Rev. Rheumatol.* **7**, 161–169. https://doi.org/10.1038/nrrheum.2010.213 (2011).

38. Terkeltaub, R., Johnson, K., Murphy, A. & Ghosh, S. Invited review: The mitochondrion in osteoarthritis. *Mitochondrion* **1**, 301–319 (2002).

Acknowledgements
We thank the patients and their families. The permissions document of the KEGG pathway database was authorized by Kanehisa laboratories.

Author contributions
Xinyu Li conducted the initial experimental design, data collection, and drafted the original manuscript.Datao Li performed additional experiments during the revision, contributed to data analysis, and made substantial revisions to the manuscript.Ruhong Zhang supervised the entire project, provided critical guidance throughout both the original submission and revision processes, and was responsible for the final approval of the manuscript.

Declarations

Competing interests
The authors declare no competing interests.

Ethics approval and consent to participate
All procedures in this research were approved by the Research Ethics Committee of Shanghai Ninth People's Hospital. The study followed the Declaration of Helsinki for ethical purposes, and all participants provided written informed consent.

Consent for publication
Written informed consent was obtained by the patient.

Additional information
Supplementary Information The online version contains supplementary material available at https://doi.org/10.1038/s41598-025-85169-x.

Correspondence and requests for materials should be addressed to D.L. or R.Z.